Proceedings of the Twenty-eighth (2018) International Ocean and Polar Engineering Conference
Sapporo, Japan, June 10-15, 2018

ISBN 978-1-880653-87-6; ISSN 1098-6189

www.isope.org

Numerical Simulations of Vortex Shedding of a Circular Cylinder Experiencing Oscillatory Flow at Low Keulegan-Carpenter Numbers

Di Deng[1], Zhe Wang[1], Decheng Wan[1], Zhiqiang Hu[2]*
[1]State Key Laboratory of Ocean Engineering, School of Naval Architecture, Ocean and Civil Engineering, Shanghai Jiao Tong University, Collaborative Innovation Center for Advanced Ship and Deep-Sea Exploration, Shanghai, China
[2]School of Engineering, Newcastle University, Newcastle upon Tyne, UK
[*]Corresponding author

ABSTRACT

In the past decades, sinusoidal motion of a circular cylinder in viscous flow had been extensively studied by researchers all around the world. While difference of flow patterns exists between fixed cylinder and freely vibrating cylinder. In this paper, numerical simulations are carried out by the in-house CFD code naoe-FOAM-SJTU with overset grid capability, which is developed based on the open source code OpenFOAM. The diameter of the cylinder is 0.02m and the KC numbers vary from 3 to 15. Results of vortex evolution, flow regimes and separation points of the cylinder with cross-flow freedom restricted and freely vibrating are compared.

KEY WORDS: Vortex shedding; Overset grid; naoe-FOAM-SJTU; KC numbers

INTRODUCTION

In actual production, the periodic oscillation of floating structures may generate relative oscillatory flow between the riser and the water. Experiments and numerical simulations of oscillatory flow around a circular cylinder have been studied by Williamson (1985), Sarpkaya (1986, 1995), Zhao et al., (2011), Graham (1980), Nehari et al., (2004), Tatsuno et al., (1990) and Obasaju et al., (1988).

Experiments of a periodically oscillated circular cylinder in still water were conducted by Williamson (1985) and Sarpkaya (1986). KC numbers ranged from 0 to 40 and flow regimes were identified within particular KC region, such as the attached vortices regime ($0<KC<7$), vortices attach to the cylinder and no shedding occurs; the single pair regime ($7<KC<15$); the double pair regime ($15<KC<24$); the three pairs regime ($24<KC<32$) and the four pairs regime ($32<KC<40$). It was found (Sarpkaya, 1986) that no separation phenomenon happened when $KC<1.1$. The Honji vortices (Honji, 1981) and separation occurred when KC number between 1.1 and 1.6. A pair of symmetric vortices generated with KC numbers ranging from 1.6 to 4. While during the region of $4<KC<7$, a pair of asymmetric vortices generated. For further KC regimes, the number of vortices pairs shed in an oscillating cycle increased by one each time the KC number changed to a higher one.

Kozakiewicz et al., (1996) and Zhao et al., (2011) conducted experiments and numerical simulations to analyze differences of the flow regimes and VIV features between a fixed cylinder and a freely vibrating cylinder in oscillatory flow. Researches were carried out at $KC=10$ and 20 with a range of reduced velocities. Kozakiewicz et al., (1996) found that the number of vortices generated in an oscillating period increased when the cylinder was freely vibrating in the cross-flow direction. Zhao et al., (2011) found that the vibration

followed different trajectories for different KC numbers and reduced velocities.
Tong et al., (2017) carried out direct numerical simulations of a square cross-section cylinder at moderate KC numbers and low Reynolds number in oscillatory flow. A map of flow regimes was formed and compared with the map of flow around an oscillating circular cylinder. Two new flow regimes were observed at KC≤2 and 10<KC<13 respectively, which were induced by the mismatch between oscillating period and the time required for vortex formulation and shedding.

In this paper, all numerical simulations are carried out by the in-house CFD code naoe-FOAM-SJTU developed by the open source platform OpenFOAM with overset grid capability. The Reynolds Averaged Navier-Stokes (RANS) equations are adopted to obtain the flow field. And the six degree of freedom equations (6DoFs) are used to compute motions of the cylinder. Firstly, the grid convergence study is conducted to verify that the solution is insensitive to the grid resolution at KC=3. Then simulations of a forced cylinder and a freely vibrating cylinder in relative oscillatory flow at KC=12 and 13.5 are conducted. Flow regimes and separation points are compared.

This paper is organized as follows: the first section gives a brief introduction to the numerical methodology. The second section presents the results of grid convergence study and simulations of KC=12 and 13.5 respectively. The final section concludes the paper.

METHOLOGY

The in-house CFD code naoe-FOAM-SJTU (Shen and Wan, 2012) is used in this paper, which is developed based on OpenFOAM combined with the overset grid program Suggar++ to calculate the cell information of the computational domian. Detailed researches have been conducted and validated by Shen and Wan (2013, 2015).

Hydrodynamic Governing Equations

In this paper, the flow field is supposed to be incompressible with constant dynamic viscosity μ and constant density ρ. The Reynolds-averaged Navier-Stokes (RANS) equations combined with SST k-ω turbulent model are used to obtain hydrodynamic response of the cylinder. The hydrodynamic governing equations are shown as followed:

$$\frac{\partial \overline{u}_i}{\partial x_i} = 0 \tag{1}$$

$$\frac{\partial}{\partial t}(\rho \overline{u}_i) + \frac{\partial}{\partial x_j}\left(\rho \overline{u}_i \overline{u}_j\right) = -\frac{\partial \overline{p}}{\partial x_i} + \frac{\partial}{\partial x_j}\left(2\mu \overline{S}_{ij} - \rho \overline{u_j' u_i'}\right) \tag{2}$$

where $\overline{S}_{ij} = \frac{1}{2}\left(\frac{\partial \overline{u}_i}{\partial x_j} + \frac{\partial \overline{u}_j}{\partial x_i}\right)$ is the mean rate of strain tensor, $-\rho \overline{u_j' u_i'}$ is referred to as Reynolds stress τ_{ij} defined as $\tau_{ij} = -\rho \overline{u_j' u_i'} = 2\mu_t \overline{S}_{ij} - \frac{2}{3}\rho k \delta_{ij}$ where μ_t is the turbulent viscosity and $k = (1/2)\overline{u_i' u_i'}$ is the turbulent energy, computed from the fluctuating velocity field.

Cylinder Motion

Fig. 1 shows a sketch of computational domain of the freely vibrating cylinder in cross-flow. The diameter of the 2D circular cylinder is D=0.02m. The rectangular computational domain is 40D in the flow direction and 30D in the cross-flow direction. The cylinder is located in the center of the domain and restrained with 4 springs of equal rigidity setting along the x-axis and y-axis. The cylinder is forced to oscillate in the flow direction(x direction) and allowed to vibrate in the cross-flow direction(y direction). The 4 springs are only active for freely vibrating cases. The displacement of the cylinder can be written as:

$$A(t) = A_m \cos(\frac{2\pi}{T}t + \varphi) \tag{3}$$

where A_m is the amplitude of the forced motion, T is the oscillating period of the cylinder, t is the time and φ is the phase angle.

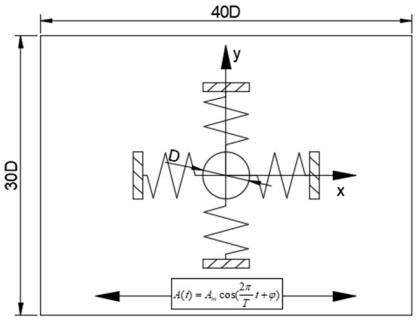

Fig.1 Sketch of the computational domain for freely vibrating cylinder

Main parameters of the cylinder are as follows: (1) the mass ratio: $m^* = m / m_d$, where m is the mass of the cylinder and $m_d = \rho g \pi D^2 / 4$ is the mass of the displaced fluid; (2) the Keulegan-Carpenter (KC) number: $KC = 2\pi \cdot A_m / D$; (3) the Reynolds number: $\mathrm{Re} = U_m D / \nu$, where U_m is the inline

oscillating velocity of the cylinder, ν is the fluid viscosity; (4) the structural damping ratio $\zeta = c/(2\sqrt{km})$, where c is the structural damping and k is the stiffness of the spring; (5) the reduced velocity $V_r = U_m/(f_{nw}D)$, where f_{nw} is the natural frequency of the cylinder in water. In all simulations, the cylinder is forced to periodically oscillate 20 cycles in the flow direction.

RESULTS

Grid Convergence Study

Firstly the grid convergence study is conducted to verify that the solution is insensitive to the grid resolution. Then the appropriate computational mesh is chosen to carry out latter simulations. The 3 meshes are shown in table 1. These three cases are in the same conditions of a fixed cylinder at KC=3.

Table1. Number of meshes for three sets of grid

	Number of mesh	Refinement ratio
Coarse mesh	0.0923M	/
Medium mesh	0.185M	1.4
Fine mesh	0.374M	1.4

Time histories of drag coefficients are shown in Fig. 2. From this figure, it has been shown that drag coefficients calculated from three meshes are very similar and errors only occur on the top and bottom points. The cause of the error may result from the complex flow field when the cylinder reverses. The meshes around the cylinder of the chosen one is shown in Fig. 3.

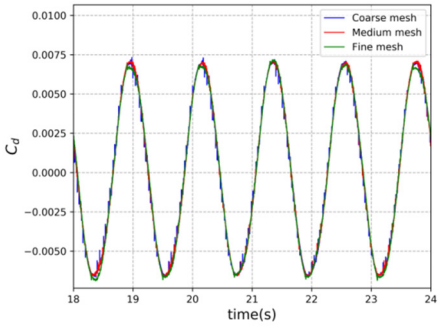

Fig.2 Drag coefficients for three sets of meshes

From previous studies of Williamson (1985) and Sarpkaya (1986), it can be known that the flow regime of the cylinder belongs to the attached vortices regime when KC=3. A pair of symmetric vortices occurs and falls out of the cylinder in each half oscillating period. While no vortex shedding happens in an oscillating period. The pair of vortices falls out of the cylinder when the cylinder reaches its rightmost or leftmost position and reverses. The flow regime of the cylinder is shown in Fig. 4. A symmetric vortex street is generated after multi-oscillating periods and a pair of symmetric vortices falls out the cylinder in each half oscillating period.

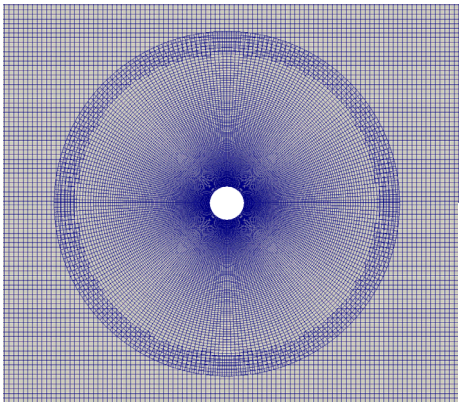

Fig.3 Computational mesh around the cylinder

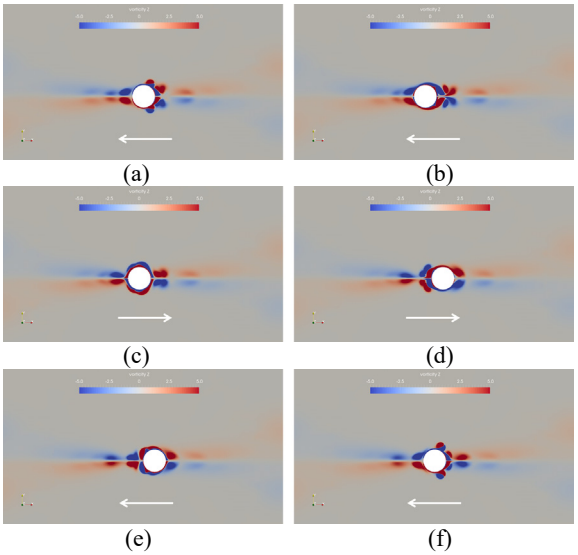

Fig.4 Vortex evolution in an oscillating period: (a) T=36.0s; (b) T=36.24s; (c) T=36.48s; (d) T=36.72s; (e) T=36.96; (f) T=37.2. Arrows refer to the direction of the cylinder motion.

Free Decay Test

In this part, the free vibration of the cylinder with an initial velocity of 0.4m/s is conducted to verify the validity of the

chosen stiffness of springs comparing with simulations of Zhao et al., (2011). The cylinder is only allowed to vibrate in the cross-flow direction. The mass ratio $m^* = 1.62$ and the structural damping ratio ζ=0.012 are referred to experiments of Kozakiewicz et al., (1996) and simulations of Zhao et al., (2011). The time histories cross-flow displacement of the cylinder is shown in Fig. 5.

The cross-flow vibration period shown in Fig. 5 is 1.26s with an error less than 3% comparing with the simulation of Zhao et al., (2011). Then the natural frequency of the cylinder is set to be 0.79Hz in this paper and the reduced velocity is 3.16 in all computational cases.

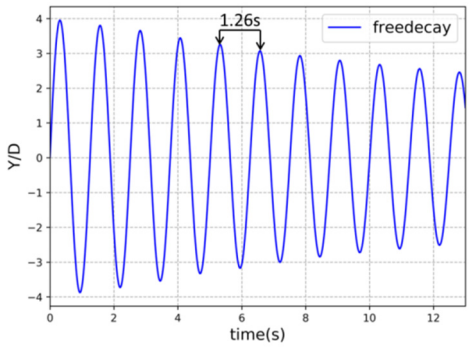

Fig.5 Free decay of a circular cylinder in still water with an initial velocity of 0.4m/s

KC=12

Fixed Cylinder

For this fixed cylinder case, the cylinder is forced to oscillate in the x direction and is not allowed to vibrate in the y direction. When KC=12, vortex shedding occurs in each half oscillating period of the circular cylinder. A pair of vortices convects away perpendicular to the motion direction of the cylinder on one side of the cylinder as shown in Fig. 6.

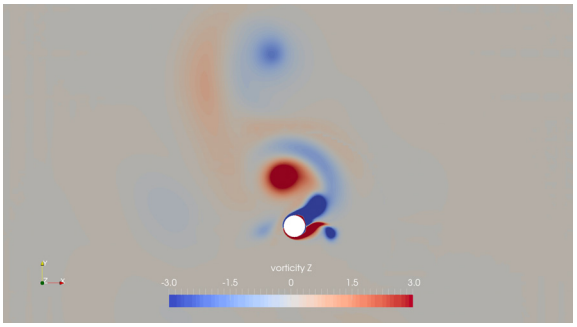

Fig.6 Vorticity graph at KC=12

Fig. 7 shows the vortex evolution in an oscillating period. When the cylinder reaches its rightmost position, a clockwise vortex "A" shown in Fig. 7(a) has been shed in the last half oscillating period. And a clockwise vortex "C" generates on the top surface of the cylinder at the same time. The anti-clockwise vortex "B" moves around the cylinder from the bottom surface to the top surface, while vortex "C" moves to the bottom during the preliminary stage of the reverse process as shown in Fig. 7(b). When the cylinder reaches its leftmost position in Fig. 7(c), the vortex "B" is intended to shed from the cylinder and the vortex "C" gets stronger during the half oscillating process. At the preliminary stage of the next half period, the vortex "B" sheds from the cylinder and gets into a group with vortex "A". And the pair of vortices convects away at around 90º to the flow direction as shown in Fig. 7(d) and Fig. 7(e). In the end of this half process, the evolution process of vortex "C" and vortex "D" is similar to vortex "A" and vortex "B" in the previous half oscillating period. In the whole oscillating cycle, two vortices convect away from the cylinder respectively in each half oscillating period. And vortex shedding only happens on one side of the cylinder.

Graphs of tangential velocity on the first layer grid of the cylinder corresponds to the vortex evolution are also shown in Fig. 7. Separation points and stagnation points of vortices are positions where tangential velocity equals 0. From Fig. 7(a) to Fig. 7(d), it can be concluded that an stagnation point is found on the front of the cylinder towards the motion direction in each half oscillating period. And the stagnation point will move around the cylinder to the opposite side of the cylinder with vortices on the cylinder surface, when the cylinder reaches the leftmost or rightmost position and begins to reverse. The appearance of separation points is always accompanied by the generating of new vortex on the cylinder's surface or vortex shedding.

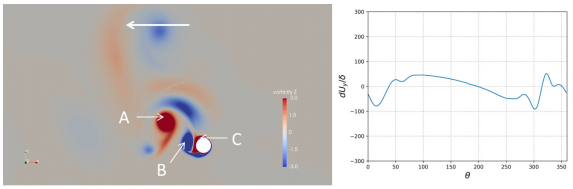

(a)

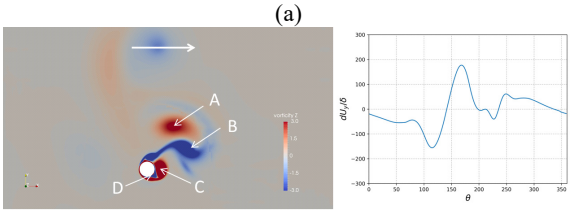

(b)

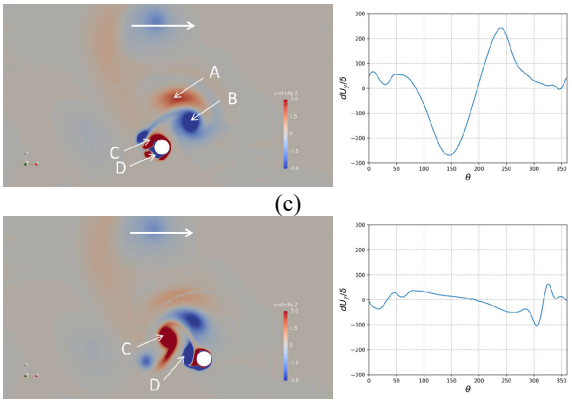

(c)

(d)

Fig.7 Vortex evolution and separation point in an oscillating period at KC=12: (a) T=75.6s; (b) T=77.2s; (c) T=78.8s; (d) T=80.4s. Arrows refer to the direction of the cylinder motion.

Freely Vibrating Cylinder

For the freely vibrating case, the cylinder is also forced to oscillate in the *x* direction as the fixed cylinder case. And the cylinder is allowed to vibrate in the *y* direction resulting from the fluctuation of pressure difference between the top and bottom side of the cylinder. Fig. 8 shows the time history of cross-flow displacement of the cylinder. Comparison on time histories of lift force coefficients between fixed cylinder and freely vibrating cylinder are shown in Fig. 9. From the comparison between time history displacement and time history of lift force coefficient of the freely vibrating cylinder, it has been shown that variations of displacement and lift force are in anti-phase. The lift force coefficient amplitude of the freely vibrating cylinder is larger than that of the fixed cylinder, which results from the cross-flow vibration.

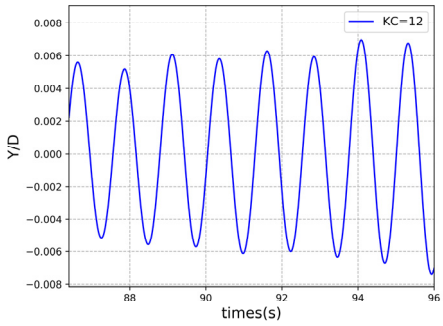

Fig.8 Time history displacement in cross-flow direction at KC=12

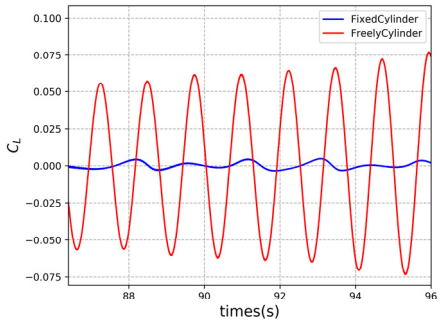

Fig.9 Time histories of lift force coefficients at KC=12

Fig. 10 shows vortex evolution process and corresponding graphs of tangential velocity on the first layer grid of the cylinder in an oscillating period. From the figure, it can be concluded that the flow regime is similar to that of the fixed cylinder. And the vortex shedding direction is perpendicular to the flow direction too. However, vortex shedding only happens on the bottom side of the cylinder, which is opposite to that of the fixed cylinder condition for the effect of cross-flow vibration.

Graphs of tangential velocity on the first layer grid of the cylinder in Fig. 10 and Fig. 7 show a degree of similarity. When the cylinder moves to its rightmost or leftmost position, changes on positions of separation points and stagnation points can be neglected on account of the small velocity and cross-flow vibration. When the cylinder moves across the center, the velocity of the cylinder reaches its maximum and the same as cross-flow vibration response, which leads to the non-negligible changes of separation points and stagnation points on the cylinder surface.

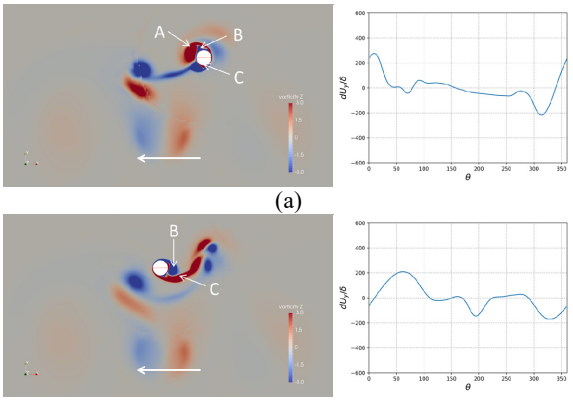

(a)

(b)

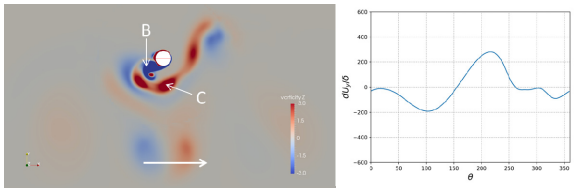

(c)

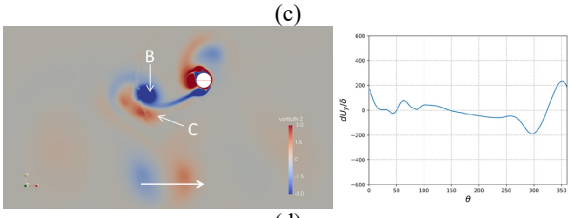

(d)

Fig.10 Vortex evolution and separation point in an oscillating period at KC=12: (a) T=75.6s; (b) T=77.2s; (c) T=78.8s; (d) T=80.4s. Arrows refer to the direction of the cylinder motion.

KC=13.5

Fixed Cylinder

For this fixed cylinder case, the cylinder is forced to oscillate in the x direction and is not allowed to vibrate in the y direction. Fig. 11 shows vortex evolution and corresponding graphs of tangential velocity on the first layer grid of the cylinder.

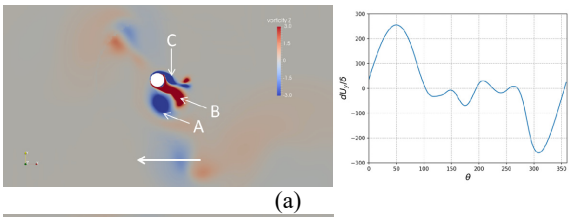

(a)

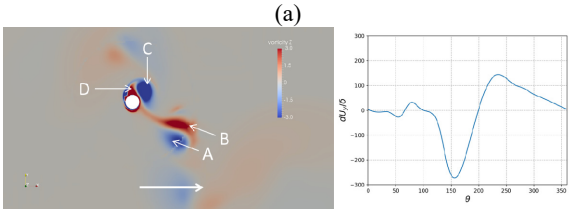

(b)

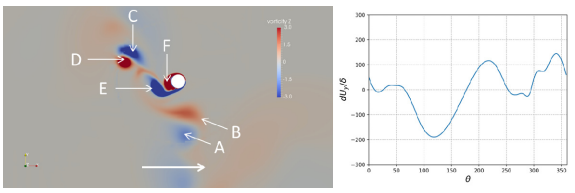

(c)

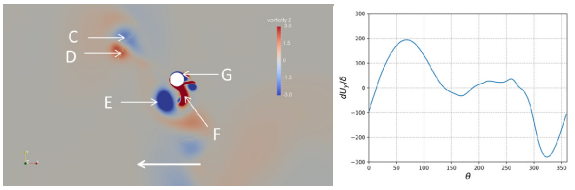

(d)

Fig.11 Vortex evolution and separation point in an oscillating period at KC=13.5: (a) T=81s; (b) T=82.6s; (c) T=84.2s; (d) T=85.8s. Arrows refer to the direction of the cylinder motion.

From Fig. 11(a) to 11(d), it has been shown that a pair of vortices sheds from the cylinder and convects away at around 45º in each half of the oscillating period. When the cylinder moves to the center of the computational domain as shown in Fig. 11(a), vortex "A" and vortex "B" come into a group with an anti-clockwise vortex "C" generating on the top side of the cylinder. Then vortex "A" and vortex "B" convect away along the bottom right direction at around 45º, when the cylinder reaches the leftmost position. During the subsequent half oscillating period, another pair of vortices, vortex "C" and vortex "D", sheds from the cylinder and convects away to the top left direction at around 45º. In the end of this period, vortex "E" and vortex "F" tend to come into a group which is similar to the phenomenon shown in Fig. 11(a).

According to graphs of tangential velocity, stagnation points still appear on the front surface of the cylinder towards the motion direction. During the reverse process, the change of stagnation point is similar to that at KC=12. And generating points of new vortices can also be confirmed through those graphs.

Freely Vibrating Cylinder

For the freely vibrating case, the cylinder is forced to oscillate in the x direction and is allowed to freely vibrate in the y direction resulting from the fluctuation of pressure difference between the top and bottom side of the cylinder. Fig. 12 shows the time history of cross-flow displacement of the cylinder. Fig. 13 shows time histories of lift force coefficients between fixed cylinder and freely vibrating cylinder. From the comparison between time history displacement and time history of lift force coefficient of the freely vibrating cylinder, it has been shown that variations of displacement and lift force are in anti-phase. However the variations of both the displacement and the lift force are irregular comparing to Fig. 8 and Fig. 9. Resulting from the cross-flow vibration, the periodical variation of lift coefficient on fixed condition changes. None obvious phase difference exists between two conditions.

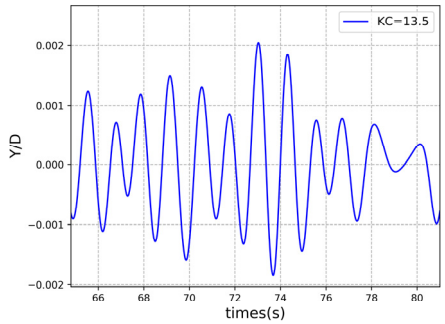

Fig.12 Time history displacement in cross-flow direction at KC=13.5

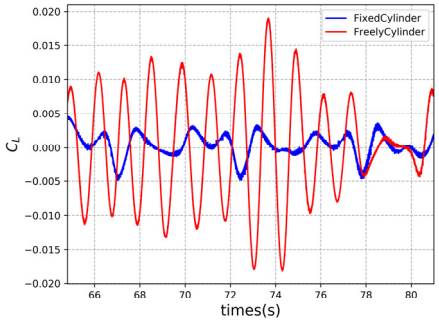

Fig.13 Time histories of lift force coefficients at KC=13.5

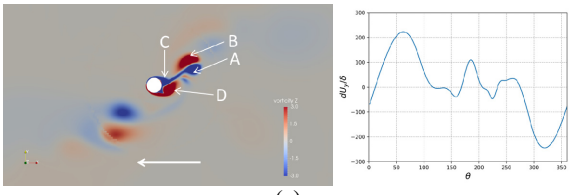

(a)

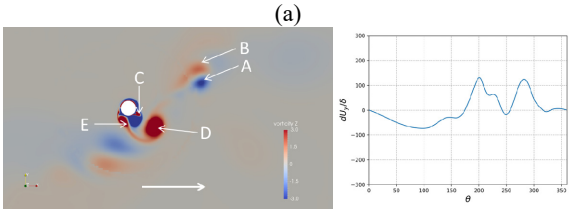

(b)

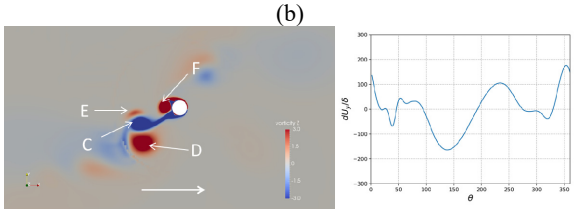

(c)

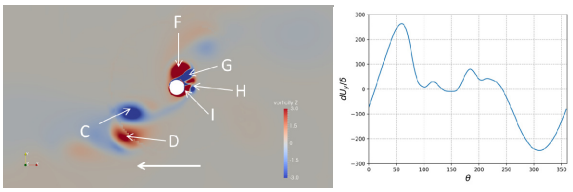

(d)

Fig.14 Vortex evolution and separation point in an oscillating period at KC=13.5: (a) T=81s; (b) T=82.6s; (c) T=84.2s; (d) T=85.8s. Arrows refer to the direction of the cylinder motion.

The vortex evolution and corresponding graphs of tangential velocity on the first layer grid of the cylinder are shown in Fig. 14. When the cylinder moves to the center of the computational domain, vortices pair of vortex “A” and vortex “B” begin to shed to the top right direction of the cylinder at around 45º. With the motion of the cylinder, the vortex “D” sheds and a small clockwise vortex “E” generates at the same time. When the cylinder reverses back to the center, the vortex “E” shed and a vortex “F” generates on the top surface. In the end of this period, vortices pair of vortex “C” and vortex “D” shed to the bottom left direction of the cylinder at around 45º, while another small anti-clockwise vortex “H” generates and sheds as the evolution of vortex “E”. Resulting from the small cross-flow displacement, tangential velocity graphs of the fixed cylinder are similar to that of the freely vibrating cylinder especially on the leftmost and rightmost positions. And obvious changes on separation points and stagnation points happen when the cylinder moves across the center of the domain, which is similar to that at KC=12.

CONCLUSION

In this paper, numerical simulations of a fixed cylinder and a freely vibrating cylinder experiencing relative oscillatory flow are carried out by naoe-FOAM-SJTU solver. Flow regimes, vortex evolution process, force coefficients and separation points are analyzed.

Results comparison show that the lift force coefficient of the freely vibrating cylinder is larger than that of the fixed cylinder condition. Phase difference exists between lift force coefficients between the fixed cylinder and the freely vibrating cylinder. From the vortex evolution process, we deduce that the vortex shedding trail changes resulting from the cross-flow vibration. When KC=12, the pair of vortices sheds from the cylinder and convects away at around 90 degree on the top side for the fixed condition and on the opposite side for the freely vibrating condition. When KC=13.5 in both conditions, a pair of vortices sheds from the cylinder and convects away at around 45 degree to the flow direction in each half oscillating period. Meanwhile a phase

difference of 90 degree exists between the trail of vortex shedding of both conditions.

Graphs of tangential velocity on the first layer grid of the cylinder show positions of separation points and stagnation points of the cylinder. Positions of new generating vortex on the cylinder can also be confirmed through these graphs.

ACKNOWLEDGEMENTS

This work is supported by the National Natural Science Foundation of China (51490675, 11432009, 51579145), Chang Jiang Scholars Program (T2014099), Shanghai Excellent Academic Leaders Program (17XD1402300), Program for Professor of Special Appointment (Eastern Scholar) at Shanghai Institutions of Higher Learning (2013022), Innovative Special Project of Numerical Tank of Ministry of Industry and Information Technology of China (2016-23/09) and Lloyd's Register Foundation for doctoral student, to which the authors are most grateful.

REFERENCES

Graham, J (1980). "The forces on sharp-edged cylinders in oscillatory flow at low Keulegan–Carpenter numbers," J Fluid Mech, 97(2), 331-346.

Honji, H (1981). "Streaked flow around an oscillating circular cylinder," *J Fluid Mech*, 107, 509-520.

Kozakiewicz, A, Sumer, BM, Fredsøe, J, and Hansen, EA (1996). "Vortex regimes around a freely vibrating cylinder in oscillatory flow," *Proc 6th Int Offshore and Polar Eng Conf*, ISOPE, Los Angeles, US, pp490-498.

Nehari, D, Armenio, V, and Ballio, F (2004). "Three-dimensional analysis of the unidirectional oscillatory flow around a circular cylinder at low Keulegan–Carpenter and beta numbers," *J Fluid Mech*, 520, 157-186.

Obasaju, E, Bearman, P, and Graham, J (1988). "A study of forces, circulation and vortex patterns around a circular cylinder in oscillating flow," *J Fluid Mech*, 196, 467-494.

Sarpkaya, T (1986). "Force on a circular cylinder in viscous oscillatory flow at low Keulegan—Carpenter numbers," *J Fluid Mech*, 165, 61-71.

Sarpkaya, T (1995). "Hydrodynamic damping, flow-induced oscillations, and biharmonic response," *J Offshore Mech and Arctic Eng*, 117, 232–238.

Shen, Z, and Wan, DC (2012). The manual of CFD solver for ship and ocean engineering flows: naoe-FOAM-SJTU. Shanghai, China, Shanghai Jiao Tong University.

Shen, Z, and Wan, DC (2013). "RANS computations of added resistance and motions of a ship in head waves," *Int J Offshore and Polar Eng*, 23(4): 263–271.

Shen, Z, Wan, DC, and Carrica, PM (2015). "Dynamic overset grids in OpenFOAM with application to KCS self-propulsion and maneuvering," *Ocean Eng*, 108: 287–306.

Tong, F, Cheng, L, Xiong, C, Draper, S, An, H, and Lou, X (2017). "Flow regimes for a square cross-section cylinder in oscillatory flow," *J Fluid Mech*, 813, 85-109.

Tatsuno, M, and Bearman, P (1990). "A visual study of the flow around an oscillating circular cylinder at low Keulegan–Carpenter numbers and low Stokes numbers," *J Fluid Mech*, 211, 157-182.

Williamson, C (1985). "Sinusoidal flow relative to circular cylinders," *J Fluid Mech*, 155, 141-174.

Zhao, M, Cheng, L, and Zhou, T (2011). "Numerical Investigation of Vortex-Induced Vibration (VIV) of a Circular Cylinder in Oscillatory Flow," ASME. *Int Conf Offshore Mech and Arctic Eng*, OMAE, Rotterdam, The Netherlands, pp 597-603.